Influence of temperature and additives on the microstructure and sintering behaviour of hydroxyapatites with different Ca/P ratios

M. A. FANOVICH, J. M. PORTO LÓPEZ
Instituto de Investigaciones en Ciencia y Tecnología de Materiales (INTEMA), (Universidad Nacional de Mar del Plata-CONICET), Av. J.B. Justo 4302 – (7600) Mar del Plata, Argentina

Sintering of two hydroxyapatite (HA) samples with different Ca/P ratios was studied as a function of thermal pretreatments, sintering temperature and additives (0–0.6 ion % Li^+ or 0–5 ion % Mg^{2+}). The samples were sintered in air and characterized by density measurements, scanning electron microscopy, differential thermal analysis, X-ray diffraction and dilatometry. Upon sintering, samples with Ca/P ratio of 1.51 (HA C) transformed to β-$Ca_3(PO_4)_2$ and $Ca_{10}(PO_4)_6(OH)_2$, resulting in materials with low densities and containing agglomerated β-$Ca_3(PO_4)_2$ when sintered above 1200 °C. Samples with a Ca/P ratio of 1.77 (HA S), without β-$Ca_3(PO_4)_2$, showed better sinterability and homogeneous microstructures. Li^+ additions favoured liquid-phase sintering and reduced the β-$Ca_3(PO_4)_2$ content in sintered materials. Mg^{2+} additions did not result in higher densities, but inhibited the hydroxyapatite grain growth rate. A significant percentage of the added Mg^{2+} was incorporated into the β-$Ca_3(PO_4)_2$ structure.

1. Introduction

Hydroxyapatite, $Ca_{10}(PO_4)_6(OH)_2$, (HA), is one of the most promising materials for the manufacture of osseous implants, because of its excellent biocompatibility, which is due to its chemical similarity with the mineral portion of hard tissues. However, the brittle nature of this ceramic limits the scope of its clinical orthopaedic and dental applications. Consequently, a great number of studies have been devoted to improving the mechanical properties of sintered calcium phosphates. At present, strengths comparable with or superior to those of human bone and tooth have been obtained using dense ceramics with or without additives [1–3].

Many investigations about hydroxyapatite have covered a wide range of compositions and experimental conditions with the aim of determining its stability limits [4]. From this point of view, the Ca/P atomic ratio is considered a particularly relevant parameter, because both mechanical properties and biodegradation rate depend on it. The Ca/P atomic ratio of stoichiometric HA is 1.67, but it can preserve its crystalline structure with Ca/P ratios as low as 1.5 [5].

The difficulties encountered in the preparation of powders with adequate morphologies to obtain HA ceramics with high densities, promoted the use of additives to modify the sintering mechanisms. In particular, Li^+ addition forms a liquid phase, which allows higher densification in materials with low green densities [2].

The objective of the present work was to study the effect of temperature and additives (Mg^{2+} and Li^+ in low concentrations) on the sintering of two HA with different Ca/P ratios, correlating these effects with the developed microstructures and to contrast some characteristics of these HA with existing data of materials containing stoichiometric Ca/P ratio (1.67).

2. Materials and methods

2.1. Starting powders

The starting materials used were a commercial (C) and a synthetic (S) HA. The commercial HA (C) (Sigma Chem. Co.) was dried at 80 °C and then ground to a powder. HA (S) was synthesized in aqueous medium by slow addition of a 0.52 M orthophosphoric acid (H_3PO_4) solution to a calcium hydroxide ($Ca(OH)_2$) suspension containing NH_4OH to maintain the pH between 12.0 and 13.0 [6]. The precipitate was aged for 24 h at 100 °C and decanted before filtering. The filtered cake was dried at 80 °C and then ground to a powder.

The particle-size distributions of these powders were determined with a Malvern 2600 size distribution analyser. The Ca/P ratio was measured by Inductively Coupled Plasma Spectrometry (ICPMS) (JOBIN-YBON, mod.JY-38). The nature of the crystalline phases present was determined by X-ray powder diffraction (XRD; Philips diffractometer with CuK_α radiation and a nickel filter, at 40 kV and 20 mA), and Fourier transform–infrared spectroscopy (FT–IR) (Bruker IFS 25) for dried and calcined samples.

0957–4530

2.2. Sample preparation and heat treatments

The powders S and C were ground in a ball mill for 1 h (samples S1, C1) and afterwards thermally treated at 500 °C (samples S2, C2) or 1000 °C (samples S3, C3) for 1 h. Furthermore, samples S2 and C2 were impregnated by the incipient wet impregnation method with $LiNO_3$ or $Mg(NO_3)_2$ solutions. The concentrations of these solutions were adjusted to obtain 0.2, 0.4 and 0.6 ion % in the case of Li^+ and 1.0, 3.0 and 5.0 ion % in the case of Mg^{2+}. The samples were calcined at 600 °C for 4 h to decompose the nitrates.

Discs of 8 mm diameter by 3–4 mm height were made by uniaxial compaction of the powders S1, S2, S3, C1, C2 and C3 in a steel mould under a pressure of 15 MPa, without binder. The green compacts were sintered in air for 1 h at 1000, 1100, 1200 and 1300 °C; the samples S2 and C2 with additives were sintered in air for 1 h at 1200 °C only. The heating schedule used was 50 °C min^{-1} up to 800 °C, 10 °C min^{-1} up to 1000 °C, and 5 °C min^{-1} up to the sintering temperature, with a hold time of 1 h at the maximum temperature. The samples were named as follows: percentage, additive (L for Li^+ and M for Mg^{2+}), kind of HA (S or C); for example, 02LC for the commercial HA with 0.2 ion % Li^+ added.

3. Results and discussion

3.1. Characterization of the samples

Chemical analysis of sample S showed a Ca/P atomic ratio of 1.77, which means an excess of calcium with respect to the stoichiometric ratio. This excess of calcium is present as free CaO. Sample C is calcium-deficient, with a Ca/P ratio of 1.51 and small quantities of carbonate ion present, as observed by FT–IR. Table I shows the phase composition of all samples after thermal treatment determined by XRD.

Particle size analysis of the starting powders revealed differences in particle size distribution, as shown in Fig. 1. Sample S has a clear bimodal particle size distribution, while C shows a single maximum at about 8 μm. However, the compacts from both samples presented similar green densities.

Dilatometric measurements on samples S and C were made with a Lhogmarny dilatometer, from room temperature to 1300 °C. The dilatometric curves showed that the shrinkage of S starts at about 800 °C, while for C it is detected at 900 °C (Fig. 2). Also, the total shrinkage exhibited by S is appreciably greater than that of C, showing that S is more reactive to sintering that C. However, it must be pointed out that calcium-deficient HA partially transforms to β-$Ca_3(PO_4)_2$ (β-TCP) at temperatures above 800 °C [5], which results in a lower global shrinkage.

TABLE I Phase composition of samples determined by XRD

Sample	Phases
S1	HA + CaO
S2	HA + CaO
S3	HA + CaO
C1	HA
C2	HA
C3	HA + β-TCP

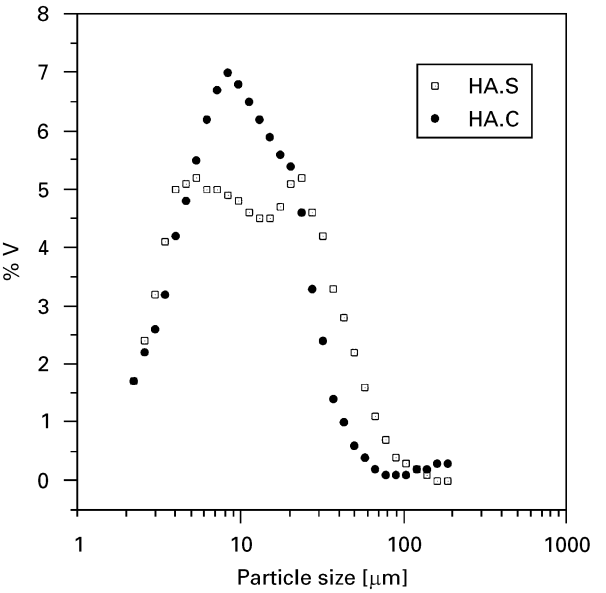

Figure 1 Particle size distributions of the starting powders.

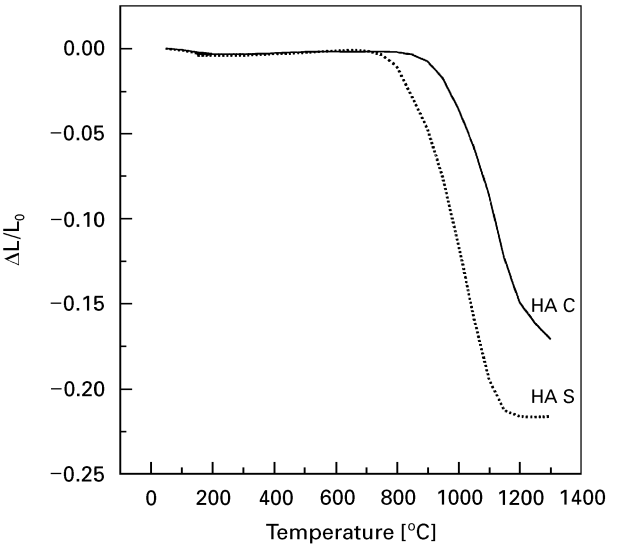

Figure 2 Dilatometric curves of samples S and C.

The thermal behaviour of both samples was also followed by differential thermal analysis (DTA; Shimadzu DTA-50H thermal analyser) up to 1400 °C, using a heating rate of 10 °C min^{-1}. The DTA thermograms are included in Figs 9 and 10, and are discussed in Section 3.3.

After sintering, the densities, phase composition and microstructure of the samples were determined. The degree of densification (apparent density and open porosity) was measured by the Archimedes' liquid-displacement method in water. The phase composition of the samples was determined by XRD.

Quantitative measurements were also made, using a HA standard synthesized in our laboratory. The standard HA was a stoichiometric HA (Ca/P = 1.67)

with a mean particle size of 25 μm, calcined at 1200 °C until constant intensity of its XRD pattern was obtained. Microstructural characterization using SEM (Philips 505) was performed on chemically etched (20 s in HCl 50% vol) fracture surfaces. Also, the degree of dispersion of MgO on the surface of the samples was determined by electron probe microanalysis (EPMA).

3.2. Effect of thermal pretreatment and sintering temperature

The densities of samples S1, S2, S3, C1, C2 and C3, sintered at 1000, 1100, 1200 and 1300 °C for 1 h are given in Fig. 3a and b.

The extent of densification strongly depends on the surface area of the starting powder; for this reason, the samples preheated at 1000 °C (S3 and C3) which are supposed to have the lowest surface area because of their greater particle size, presented the lowest apparent density after sintering. Samples of series 1 and 2 showed a homogeneous microstructure, resulting in high densities.

The β-TCP phase present in the samples C after thermal treatments has a marked tendency to agglomerate, which increases with temperature, and is therefore most notable on preheating at 1000 °C.

The densification of both series of samples followed a rather similar trend, as shown in Fig. 3a and b.

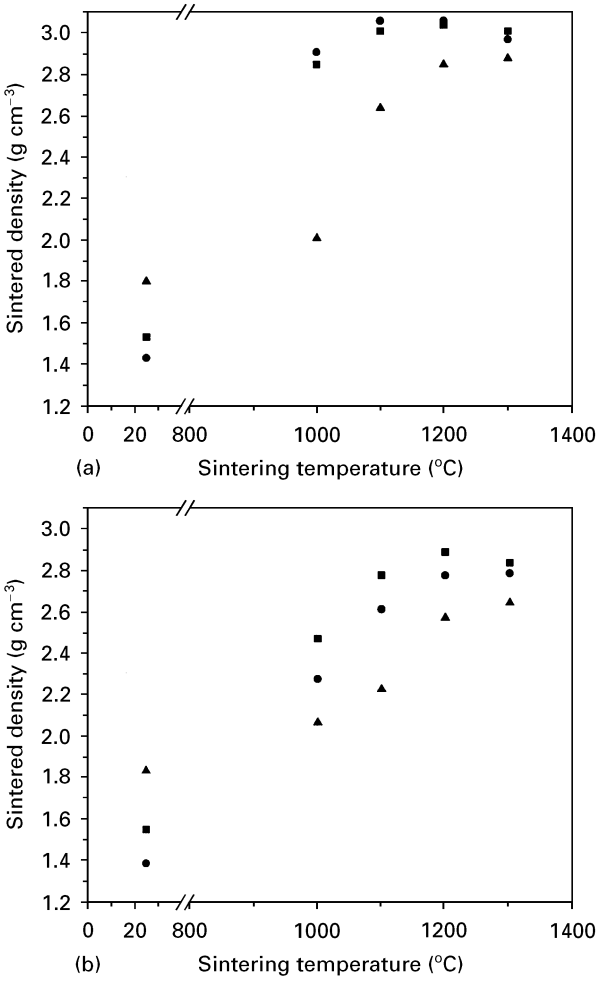

Figure 3 Sintered density versus temperature curves for series (a) S, and (b) C. (■) S1, C1; (●) S2, C2; (▲) S3, C3.

However, the density–temperature curves reached a plateau at about 1100 °C for the samples S and at about 1200 °C for the samples C. This fact is in agreement with the dilatometric analyses, in which S began to contract at a temperature lower than that of C.

Both samples showed similar green densities; however, S2 reached a higher sintered density than C2 and began to contract at lower temperatures. This effect may be attributed to an advantageous grain size distribution, and to the absence of β-TCP as second phase, which probably had an important role on the densification of C2.

Samples S1 and S2 increased their densities in a relatively narrow temperature range, reaching the maximum density at about 1100 °C, whereas C1 and C2 increased their density in a gradual way. The end of the densification or even a slight density decrease observed at higher temperatures (1300 °C) may also be due to the partial decomposition of HA. For samples S1 and S2, the increase of sintering temperature from 1000–1300 °C improves the homogeneity and favours grain growth, resulting in an increase in mean grain size from approximately 0.2 μm to 2–4 μm; Fig. 4 shows this effect on S2.

This increase in grain size is more important as Ca/P decreases, and the samples containing β-TCP (C1 and C2) presented abnormal grain growth. Table II lists the grain sizes, D, of samples S1 and C1 as a function of sintering temperature. On the other hand, micrographs of sintered C samples revealed significant microstructural changes: at 1200 °C the microstructure is heterogeneous, the smaller grains probably corresponding to the β-TCP phase [7]. A conclusive identification of the different phases (HA and TCP) could not be made by electron microprobe analysis.

The activation energy for grain growth can be calculated from the plot of $\ln D$ versus $1/T$ for a constant sintering time for the data in Table III. The calculated values were compared with those reported by Jarcho *et al.* [8] and Van Landuyt *et al.* [9]. Sample C showed an activation energy similar to sample A and B from literature data, while S had a significatively lower value. This may be due to the better sintering behaviour of S, as previously described, more than a compositional variation in the samples. In this way, these characteristics allowed high densifications to be reached without exaggerated grain growth.

3.3. Sintering of powders with additives

According to the sintering results obtained with different preheating treatments, S2 and C2 were selected to study the effect of additives.

3.3.1. Sintering of HA powders with Li^+

The densities of compacts S2 and C2 sintered for 1 h in air at 1200 °C with 0.2, 0.4 and 0.6 ion % Li^+, respectively, are given in Fig. 5, as a function of Li^+ concentration. The initial stage of sintering of hydroxyapatite with lithium at 1200 °C is promoted by a liquid phase

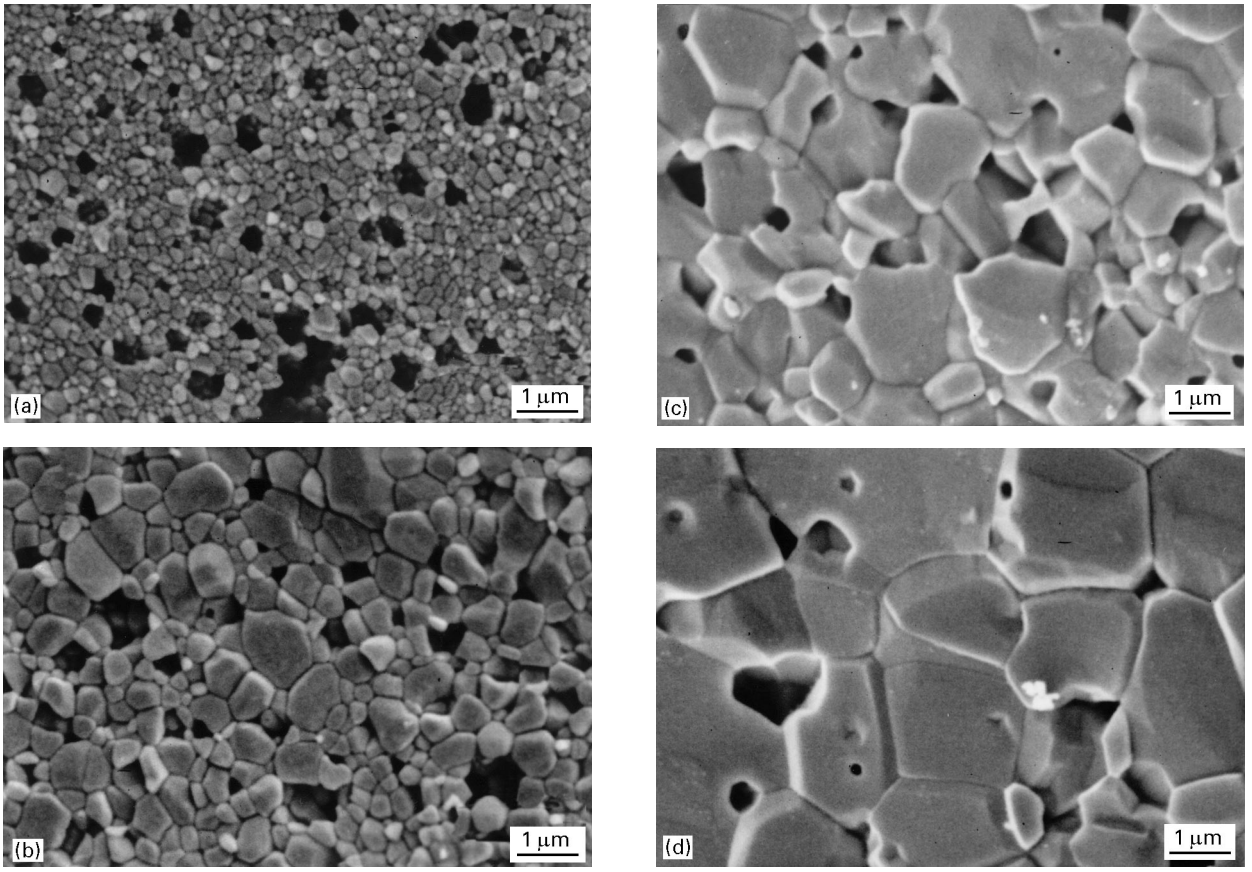

Figure 4 Scanning electron micrographs of sample S2 sintered at (a) 1000 °C, (b) 1100 °C, (c) 1200 °C, (d) 1300 °C.

TABLE II Grain size of samples S1 and C1 as a function of sintering temperature

Samples	1000 °C	1100 °C	1200 °C	1300 °C
S1	0.2	0.5	1.0	2.0
C1	0.5	1.1	13.0	> 13.0

TABLE III Activation energy for grain growth as function of Ca/P ratio

Sample	Ca/P	Activation energy (kcal mol^{-1})
S1	1.77	28
C1	1.51	50
A [9]	1.68	47
B [8]	–	56

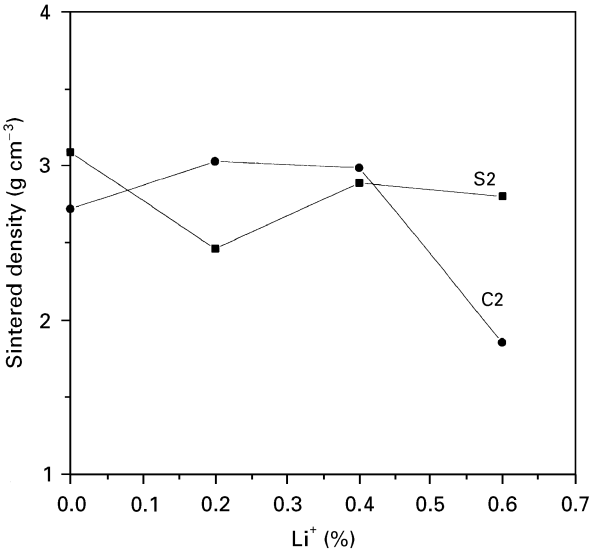

Figure 5 Sintered density versus Li^+ concentration for samples S2 and C2.

[2]. The presence of liquid phase was observed by SEM on samples without chemical etching.

The sample 02LC developed a slightly coarser but homogeneous microstructure, reaching a relative density of 96%. Higher Li^+ additions resulted in appreciable grain growth and open porosity (04LC), while for 06LC, a dramatic density decrease to 59%, with much greater pores, was observed (Fig. 6). The grain growth observed for 04LC, which was less pronounced than that of the series S, did not result in this case in a decrease of density, because the effect of the liquid phase prevailed on densification more than on grain growth.

The decrease in density of S with 0.2 ion % Li was due to an extraordinary grain growth (Fig. 7), which left many trapped pores. With higher concentrations of Li^+, which provided more liquid phase, the grain growth was not so important, and the faster material

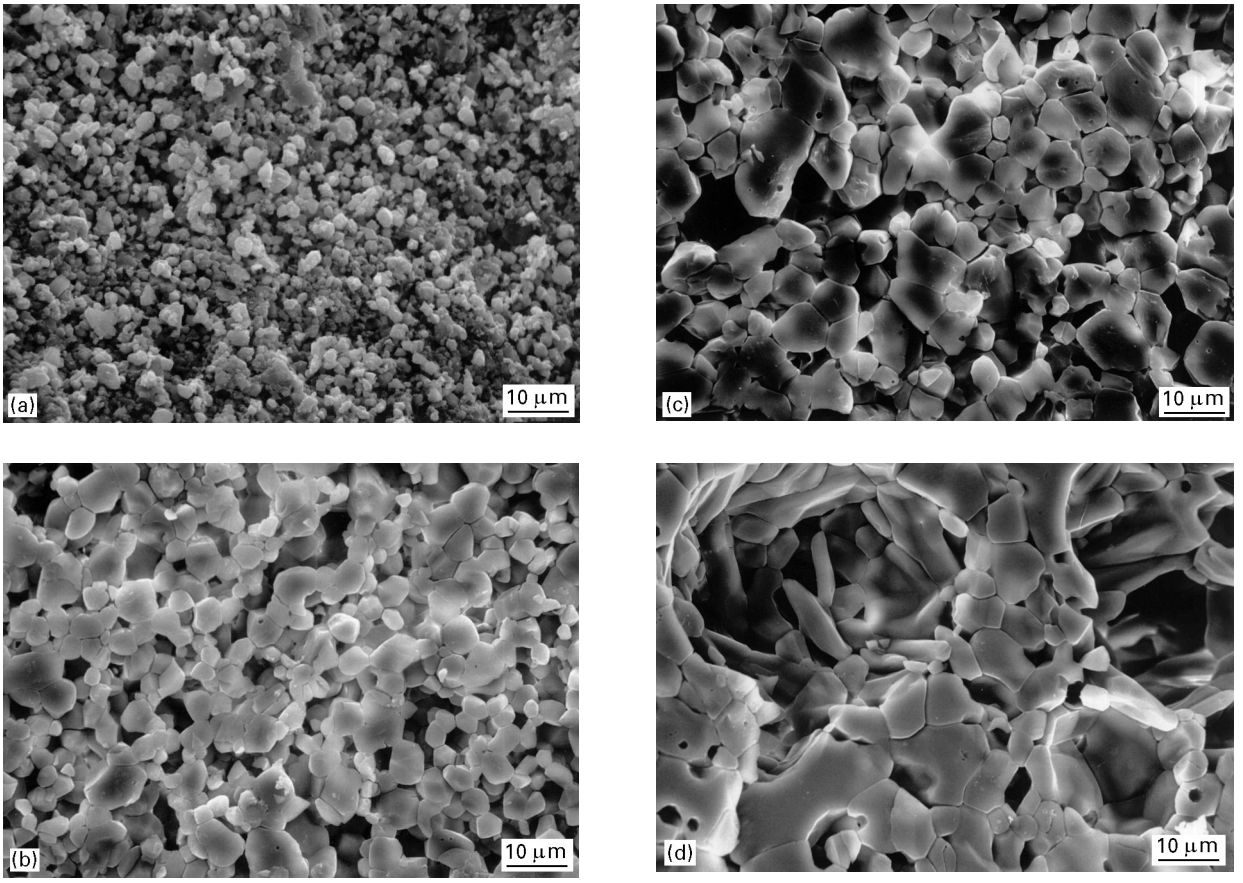

Figure 6 Scanning electron micrographs of sample C2, (a) without Li^+, (b) 0.2% Li^+, (c) 0.4% Li^+, (d) 0.6% Li^+.

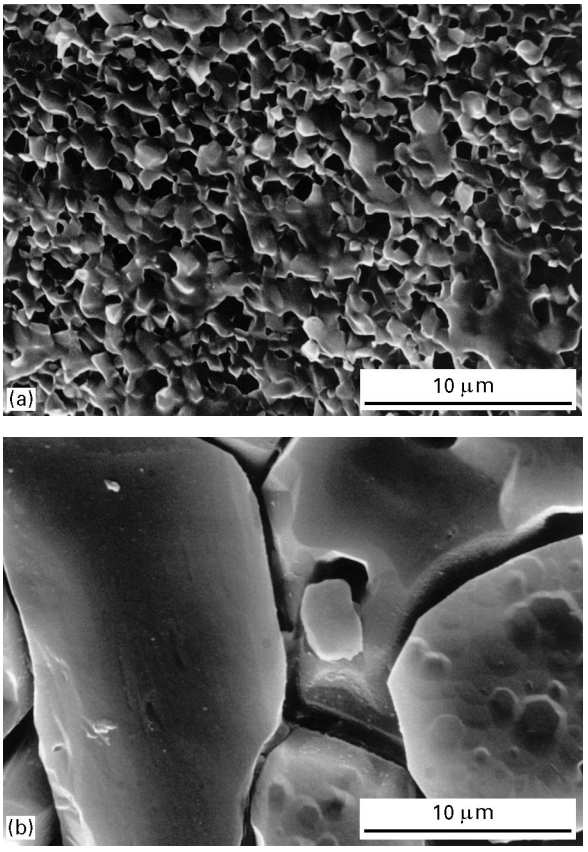

Figure 7 Scanning electron micrographs of samples (a) S2 and (b) 02LS.

transport resulted in an increase in density, reaching about 90% for 04LS and 06LS.

It must be noted that the quantity of liquid phase in samples S, detected by SEM, which have less soluble material, is lower than in samples C. Also, the formation of a greater quantity of liquid in C extends over a broader temperature range.

Furthermore, XRD analyses of series C showed that the β-TCP content for Li^+ additions between 0% and 0.6% decreases from 14% to 9%, this difference contributing to liquid-phase formation. The presence of the liquid phase is suggested by the existence of a eutectic point between Li_3PO_4 and $Ca_3(PO_4)_2$ at 1010 °C [2]. At the sintering temperatures used, the presence of a glass network modifier (Li^+) results in the formation of a phosphate glassy phase. This was confirmed by SEM observations of samples with and without chemical etching (see Fig. 8). Also, evidence of the presence of a non-crystalline phase was found by electrical measurements [10]. The diminution of β-TCP content could be due to a greater solubility of TCP than HA in the liquid phase. For the series S with lithium, the Ca/P ratio of the crystalline phase is high enough to maintain the hydroxyapatite structure at low Li^+ additions (0.2% and 0.4%). However, XRD analysis of sample 06LS shows the presence of small quantities of β-TCP; this agrees with previous studies [2] in which it is reported that the partial decomposition of HA to β-TCP increases with greater Li^+

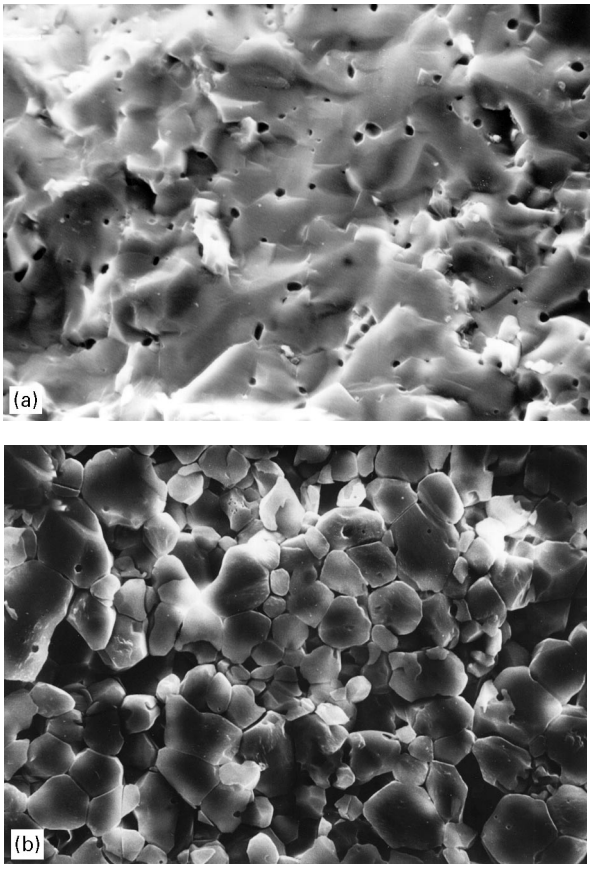

Figure 8 Scanning electron micrographs of samples (a) 04LC without chemical etching and (b) 04LC with chemical etching.

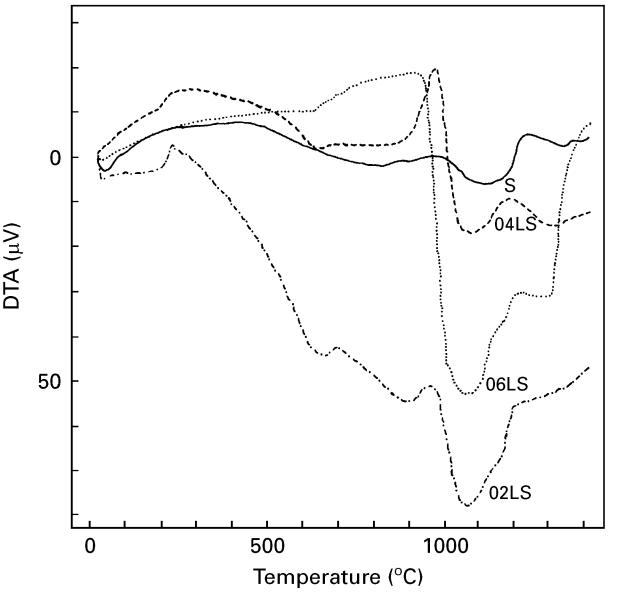

Figure 9 Differential thermal analyses of samples S with lithium.

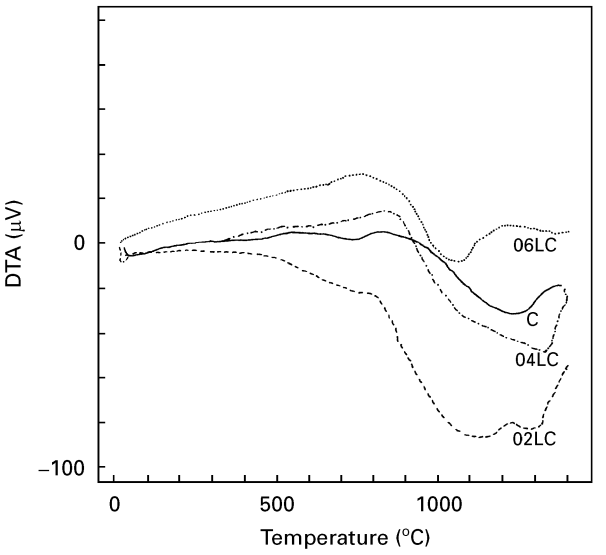

Figure 10 Differential thermal analyses of samples C with lithium.

additions. Then, in the calcium-deficient HA, a partial decomposition to β-TCP takes place at $T > 700\,^{\circ}C$ even in absence of Li^+, while for stoichiometric HA phase, the apatitic structure is stable at these temperatures as long as there is no liquid phase present.

The DTA diagrams of series S (Fig. 9) show broad exothermic bands starting at about 650 °C, due to HA crystallization. Also, endothermic effects appear at higher temperatures (900–1000 °C), which are attributed to liquid-phase formation. The temperature of liquid-phase formation decreases with increasing Li^+ additions.

The DTA diagrams of series C are given in Fig. 10. The HA crystallization bands are not so evident as in series S; instead, an endothermic band, due to partial decomposition of HA to β-TCP, is observed at about 700 °C. This band is less intense for the lithium containing samples; this fact is in accordance with the β-TCP contents determined by quantitative XRD analyses of the samples sintered at 1200 °C. As in series S, the formation of liquid phase is observed, starting at 750–900 °C; again this temperature decreases with higher Li^+ concentrations.

3.3.2. Sintering of HA powders with Mg^{2+}

In Fig. 11, the densities and open porosities, P_0, of both series of samples are plotted as a function of Mg^{2+} content. The addition of Mg^{2+} to the samples of series S had no appreciable effect on density or open porosity, although the latter slightly increased with 5% Mg^{2+}. SEM observations and EPMA analyses showed a heterogeneous distribution of magnesium along this series, with MgO clusters on the surfaces (Fig. 12).

The temperature at which the crystallization of HA starts, increased with Mg^{2+} concentration; this fact is in accordance with previous studies, reporting the inhibiting effect of Mg^{2+} on HA crystallization [5].

For series C, a density increase was observed only with 1% Mg^{2+}; at the same time, the porosity was reduced to 50% of that of the original sample. With higher Mg^{2+} contents, the density is lower, and correspondingly the porosity increases. The Mg^{2+} distribution also differs from that of the S series. In this case, the dispersion is much more homogeneous, and the relatively large MgO clusters are not observed. This observation may be related to the presence of β-TCP in this series, and the substitution of Mg^{2+} for Ca^{2+} in its structure [11].

The differential thermal analyses of the samples C and 1MC show an endothermic band starting at about 700 °C, due to the decomposition of calcium-deficient HA into stoichiometric HA and β-TCP. This band is not present in the DTA diagrams of the samples 3MC and 5MC. As will be discussed in the following paragraphs, this corresponds with the relative β-TCP content, determined by XRD.

To check for the possible incorporation of Mg^{2+} in the crystalline structure of HA and/or β-TCP, XRD measurements were made on both series of samples. The positions of the HA peak at 31.7° 2θ and the β-TCP peak at 31.1° 2θ, as well as the free MgO content (peak at 42.4° 2θ) were determined for all the samples. As the free MgO contents are low, the last determination was affected by a large relative error; however, it still indicated that an appreciable fraction of the total added Mg^{2+} was incorporated into the β-TCP lattice. The obtained results are given in Table IV.

As the percentage of added Mg^{2+} increases up to 3%, the β-TCP content decreases to approximately 60% of the initial concentration. At the same time, the intensity of the HA peak is not affected by the Mg^{2+} additions. Also, the constant angular position of the HA peak indicates that Mg^{2+} was not incorporated into its structure, under the experimental conditions used.

The interplanar spacing $d_{(0.2,10,2\bar{1}7)}$ [12] of β-TCP slightly decreases in the sample 5MC, confirming that part of the added Mg^{2+} is incorporated to the β-TCP structure [13]. It has been reported [14] that $Mg_3(PO_4)_2$ dissolves in $Ca_3(PO_4)_2$ up to 12% by weight at 1200 °C. Also, these results correlate well with the effects due to β-TCP observed by thermal analysis.

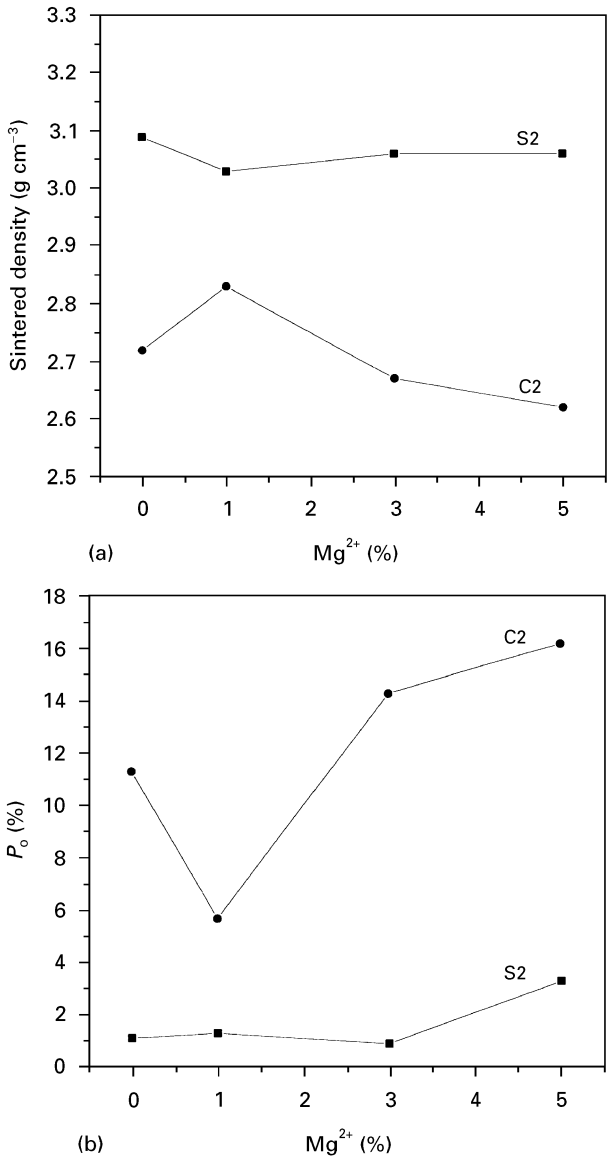

Figure 11 (a) Sintered density and (b) porosities versus Mg^{2+} content for samples S2 and C2.

4. Conclusions

During sintering of a commercial calcium-deficient HA, partial transformation to β-TCP and agglomeration of this phase were observed at high temperatures. This led to the production of heterogeneous microstructures, accompanied by enhanced grain growth of HA. Precalcination at 1000 °C seems to favour β-TCP agglomeration. Furthermore, it reduces the surface area, resulting in lower densifications and in the production of interconnected porosity.

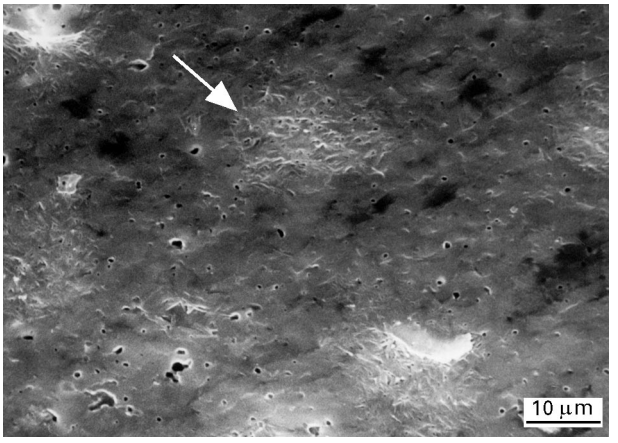

Figure 12 Scanning electron micrograph of sample S2 showing MgO clusters.

TABLE IV Compositions and *d*-spacing measurements for series C with added Mg^{2+}

Sample	Free MgO (%)	TCP 2θ (deg)	*d* (nm)	TCP (%)	HA 2θ (deg)	*d* (nm)	HA (%)
C	–	31.12	0.287	14.0	31.73	0.282	86.0
1MC	0.5	31.15	0.287	10.0	31.72	0.282	89.5
3MC	2.1	31.12	0.287	9.0	31.71	0.282	88.9
5MC	2.8	31.21	0.286	9.0	31.74	0.282	88.2

In spite of the similar green densities, HA samples without β-TCP showed better sinterability and produced more homogeneous microstructures, with intergranular pores having diameters of about 1 μm. This may be attributed not only to the chemical composition (absence of β-TCP), but also to the different size distribution of the starting powders. The controlled stoichiometry and the appropriate grain-size distribution allow the achievement of high densities (97%–98%) after sintering at 1200 °C in air.

The effect of additives as modifiers of the sintering process was more important on calcium-deficient HA. Li^+ additions resulted in liquid-phase sintering, as observed by SEM and electrical measurement [10]. The liquid phase is supposed to be a Li^+ and Ca^{2+} phosphate glassy phase. The formation of liquid phase reduced the β-TCP content in the sintered materials, because it dissolves in the glassy phase. The highest Li^+ percentage (0.6%), resulted in pores 50–60 μm in diameter in samples with β-TCP.

Mg^{2+} additions did not result in higher densities, nor in significant changes in HA and β-TCP contents. However, the developed microstructures showed that Mg^{2+} slows down the grain growth of HA. A significant part of the added Mg^{2+} was incorporated into the crystalline structure of β-TCP in the experimental conditions used. Furthermore, Mg^{2+} distribution was much more homogeneous in calcium-deficient HA than in stoichiometric HA, which does not contain β-TCP.

References

1. P. E. WANG and T. K. CHAKI, *J. Mater. Sci. Mater. Med.* **4** (1993) 150.
2. T. GOTO, N. WAKAMATSU, H. KAMEMIZU, M. IIJIMA, Y. DOI and Y. MORIWAKI, *J. Mater. Sci.* **26** (1991) 149.
3. A. J. RUYS, C. C. SORRELL, A. BRANDWOOD and B. K. MILTHORPE, *J. Mater. Sci. Lett.* **14** (1995) 744.
4. K. DE GROOT, C. P. A. KLEIN, J. G. C. WOLKE and J. M. A. DE BLIECK-HOGERVORST, in "Handbook of Bioactive Ceramics", Vol. II, edited by T. Yamamuro, L. L. Hench and J. Wilson (CRC Press, Boca Raton, FL, 1990) pp. 7–9.
5. A. RAVAGLIOLI and A. KRAJEWSKI, "Bioceramics" (Chapman and Hall, London, 1992) p. 176.
6. H. AOKI, "Medical Applications of Hydroxyapatite" (Ishiyaku EuroAmerica, Tokyo, 1994) p. 176.
7. A. ROYER, J. C. VIGUIE, M. HEUGHEBAERT and J. C. HEUGHEBAERT, *J. Mater. Sci. Mater. Med.* **4** (1993) 76.
8. M. JARCHO, C. H. BOLEN, M. B. THOMAS, J. BOBICK, J. F. KAY and R. H. DOREMUS, *J. Mater. Sci.* **11** (1976) 2027.
9. P. VAN LANDUYT, F. LI, J. P. KEUSTERMANS, J. M. STREYDIO, F. DELANNAY and E. MUNTING, *J. Mater. Sci. Mater. Med.* **6** (1995) 8.
10. M. A. FANOVICH, M. S. CASTRO and J. M. PORTO LÓPEZ, *Mater. Lett.*, in press.
11. P. G. GALLIANO and J. M. PORTO LÓPEZ, in "Proceedings of the XVI International Congress on Glass", Vol. 5, edited by A. Duran and J. M. Fernández Navarro, (Sociedad Española de Cerámica y Vidrio, Madrid, 1992) pp. 75–80.
12. International Centre for Diffraction Data, Data Card 9–169 (Philadelphia, 1967).
13. D. FISHER, *Am. Mineral.* **45** (1960) 645.
14. E. M. LEVIN, C. R. ROBBINS and H. F. McMURDIE, "Phase Diagrams for Ceramists", Vol. 1 (The American Ceramic Society, Columbus, OH, 1964) p. 214.

Received 6 August 1996
and accepted 15 July 1997